

Article

Comparative Study of the Performance of Underwater Concrete between Anionic and Nonionic Anti-Washout Admixtures

Xiaoyun Song ¹, Heping Zheng ², Lei Xu ^{1,*}, Tingting Xu ¹ and Qiuyu Li ¹

¹ Qingdao Institute of Marine Geology, China Geological Survey, Qingdao 266071, China; sxy854234635@163.com (X.S.)

² Department of Civil Engineering, Qingdao University of Technology, Qingdao 266033, China

* Correspondence: xulei2014107@163.com

Abstract: An investigation was carried out to study the influence of two types of anti-washout admixtures (AWAs) on the performance of underwater concrete, specifically, workability and washout resistance. The tested AWAs were hydroxypropyl methylcellulose (HPMC) and polyacrylamide (PAM) as nonionic AWAs and carboxymethyl starch (CMS) and polyanionic cellulose (PAC) as anionic AWAs. Rheological properties (slump and slump flow), washout resistance, and compressive strength were measured to evaluate the properties of the fresh and hardened concrete. The results indicate that anionic AWAs are more effective at improving workability and strength than nonionic AWAs in anti-washout underwater concrete. When the nonionic AWA dosage exceeded 0.3% (W/C = 0.45), the fluidity and air content were negatively impacted. Additionally, nonionic AWAs more readily alter the morphological structure of cement paste, affecting cement particle hydration and underwater concrete properties. Regarding the mechanical properties, compared with those of concrete without AWAs and with nonionic AWAs, the 28-day compressive strength of concrete with anionic AWAs reached 37 MPa, an increase of 151% and 131%, respectively. Compared with nonionic AWAs, concrete with anionic AWAs is more stable.

Keywords: anti-washout admixture; underwater concrete; anionic; nonionic



Citation: Song, X.; Zheng, H.; Xu, L.; Xu, T.; Li, Q. Comparative Study of the Performance of Underwater Concrete between Anionic and Nonionic Anti-Washout Admixtures. *Buildings* **2024**, *14*, 817. <https://doi.org/10.3390/buildings14030817>

Academic Editor: Cedric Payan

Received: 13 February 2024

Revised: 9 March 2024

Accepted: 15 March 2024

Published: 17 March 2024



Copyright: © 2024 by the authors. Licensee MDPI, Basel, Switzerland. This article is an open access article distributed under the terms and conditions of the Creative Commons Attribution (CC BY) license (<https://creativecommons.org/licenses/by/4.0/>).

1. Introduction

Underwater concrete construction presents significant challenges due to the washout of cementitious materials and loss of workability. Anti-washout admixtures (AWAs) are commonly used to enhance the cohesion and washout resistance of underwater concrete [1]. AWAs can be categorized as nonionic (e.g., HPMC, PAM) or anionic (e.g., PAC, CMS), depending on their ionic nature. Nonionic AWAs utilize hydrogen bonding and entanglement to increase viscosity and reduce washout [2]. Anionic AWAs utilize charge neutralization and interparticle bridging. While both types increase cohesion, their effects likely differ. This study aimed to compare the effects of nonionic and anionic AWAs on key properties of underwater concrete, including its workability, washout resistance, strength development and microstructure. Expanding the understanding of AWA mechanisms will enable more optimized specifications and designs of underwater concretes [3,4].

Underwater concretes will be prepared with two concentrations of nonionic AWAs (HPMC and PAM) and two concentrations of anionic AWAs (PAC and CMS). Workability will be assessed via slump flow and viscosity measurements [5]. The compressive strength development will be measured at standard curing ages. Microstructural characteristics will be examined by scanning electron microscopy (SEM) to visualize flocculation mechanisms [6].

It is hypothesized that nonionic AWAs will provide superior workability retention but potentially inferior strength development compared to anionic alternatives. Anionic AWAs are expected to show higher washout resistance, attributable to their stronger interparticle bonding [7–9]. Both classes are expected to demonstrate flocculation and viscosity

enhancements relative to plain underwater concrete, but potentially through disparate mechanisms that are observable at the microscale. In conjunction with the experimental program, molecular dynamics (MD) simulations will be performed to elucidate AWA–cement–water intermolecular interactions at the nanoscale and microscale [10,11]. These simulations can solve Newton’s equations of motion for matrix components to determine atomic trajectories and reveal transient binding phenomena [12,13].

Both nonionic and anionic AWA polymer chain configurations will be constructed within representative cement pore fluid models under shear flow. Nonbonded interaction parameters will be assigned between chain atoms and ionic species per the established force field [14]. Transport properties such as shear viscosity and self-diffusion coefficients will be extracted from the model to correlate with rheology tests. Particle residence times near polymer chains will provide further evidence of flocculation tendencies. Simulations will also probe the differences between intrachain hydrogen bonding for nonionic polymers and interchain ionic bonding for anionic variants [15–18]. The extent, duration, and dynamics of these atomic interactions are expected to govern macroscale washout resistance behavior. Sensitivity analyses will map the bonding affinity with the polymer charge density, molecular weight, and shear rate [19].

By connecting molecular configurations and kinetics to bulk phenomena, the simulations will offer unique insights into AWA mechanisms that are difficult to capture experimentally [20,21]. The visualization and quantification of transient binding dynamics will support the interpretation of bulk property measurements. The models can also be used to screen AWA molecular architectures to guide the design and synthesis of next-generation admixtures [22]. This work provides a side-by-side quantitative comparison between nonionic and anionic AWAs regarding key underwater concrete performance attributes. An enhanced understanding of the governing mechanisms will help concrete specialists select suitable AWAs tailored to specific application requirements [23–25]. Characterizing the interactions between distinct AWA chemistries and cement systems will enable further material innovations and structural applications of underwater concrete.

2. Experimental Sections

2.1. Materials

All the AWAs and equipment were received from Qingdao Kremer New Building Materials Technology Co., Ltd., Qingdao, China. The degree of substitution (DS) was above 0.2 for CMS. The apparent viscosity of PAC was 15 mPa·s. The surface tension of the 2% HPMC solution ranged from 42 to 56 dyn·cm^{−1}. The average molecular weight of PAM was 5,000,000–6,000,000. All chemicals used were of analytical grade [26].

Shanshui 42.5 Portland cement with a blade fineness of 311 m²/kg was utilized to prepare the concrete test specimens used for determining the concrete properties. The chemical composition of the cement is shown in Table 1. The water reduction rate was 40% for the polycarboxylate superplasticizer.

Table 1. Chemical composition of the studied cement.

CaO	SiO ₂	Al ₂ O ₃	Fe ₂ O ₃	MgO	SO ₃	K ₂ O	Na ₂ O	P ₂ O ₅	CaO Free	Ignition Loss
55.85%	22.91%	7.12%	3.36%	3.28%	2.30%	0.69%	0.22%	0.19%	1.25%	1.44%

2.2. Mixing Procedures and Concrete Mix

The mixing protocols and processes have a large influence on the fluidity and workability of UWC, particularly when AWAs and superplasticizers are added. Potential chemical and physical interactions, such as cement hydrates, the adsorption of superplasticizers, and AWA crosslinking in UWCs, will be greatly affected [27]. When AWAs and superplasticizers are mixed with cement mortar slurry, the cement particles are wrapped by AWAs, so the amount of superplasticizer that is adsorbed decreases, which results in a slow setting [28].

To maximize the synergy and combination of admixtures, and limit experimental errors, the mixing procedure was performed as follows:

Step 1: All the cement and coarse and fine aggregates were dry-mixed for 1 min.

Step 2: The water and superplasticizer were mixed to the solution. The solution was added to the mixture uniformly within 30 s while stirring for 2 min.

Step 3: The AWAs were added to the mixtures and stirred for 1 min.

The stirring speed was $42 \text{ r}\cdot\text{min}^{-1}$, and the UWC was mixed without stopping.

In the mixing process, nonionic AWAs generate many bubbles in concrete, which are not conducive to sinking of the UWC.

2.3. Cement Mortar Test

2.3.1. Fluidity and Fluidity Loss

The fluidity of cement mortar can not only reflect the viscosity and washout resistance of the UWC but can also reflect the workability and fluidity loss as a reference [29]. Thus, to study the fluidity and fluidity loss of different UWCs, cement mortar was tested to determine the optimal dosage of AWAs [30].

Standard sand was used in the test, and the W/C was 0.5 [31–33].

With an increase in the dosage of AWAs from 0 to 1.2% (Figures 1 and 2), the fluidity of the cement mortar sharply decreases, especially at low dosages. However, the decrease in the fluidity of the mortar with nonionic AWAs is significantly greater than that with ionic AWAs. In addition, the fluidity loss after two hours shows that there is an opposite trend in fluidity loss between the two kinds of AWAs before a dosage of 0.9%, and the fluidity loss with CMS is relatively lower and more stable [34]. Additionally, the fluidity loss of UWC with AWAs was even less than that of non-AWA UWC at some dosages, which indicated that AWAs retain water in UWC and reduce fluidity loss, or that the fluidity of UWC is so low that it reaches the lower limit. In practical tests, when the dosage of nonionic AWAs reaches 0.9%, the cement mortar is too sticky to meet the fine workability requirements of UWC; thus, the dosage of AWAs is limited to between 0.1 and 0.6% in UWC [35]. According to the fluidity test, the average fluidity decreases by 45.1% and 37.5% with the use of nonionic and anionic AWAs, respectively, which shows that anionic AWAs have a less negative impact on the flow properties of concrete [36,37].

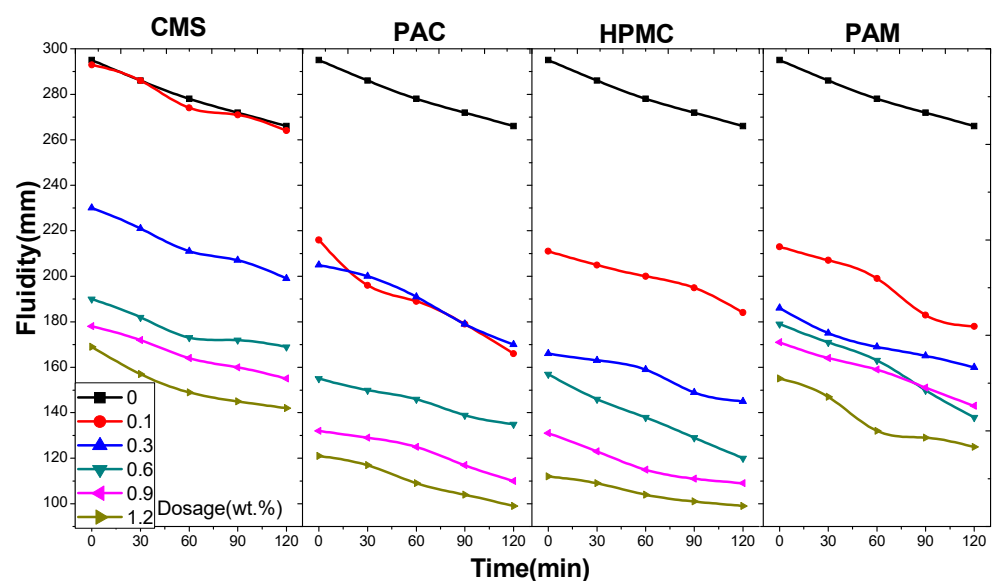


Figure 1. Fluidity and fluidity loss of cement paste with CMS, PAC, HPMC, and PAM.

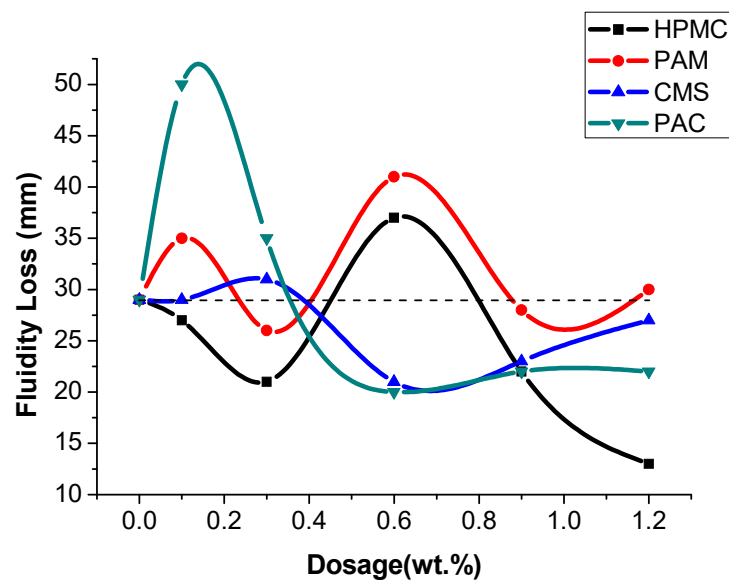


Figure 2. The fluidity loss after two hours.

2.3.2. pH Factor Test and Stream Test

Considering the greater impact of coarse aggregate on the test results, the anti-washout resistance was tested with mortar. A 100 g sample of cement mortar was added to a beaker containing 300 mL of water. After 3 min of precipitation, most of the sediments sank to the bottom. The pH factor test has been proposed for determining the washout resistance of UWC in Japan [1]. However, the flocculating states significantly differ between AWAs alone and mortar without AWAs [38]. The interfaces between the supernatant and suspension were not obvious, and the concentrations of the suspensions also differed (Figure 3). Thus, separating the supernatant solution from the suspension is difficult, and this phenomenon leads to instability and inaccuracy in the pH factor test. Finally, the pH of the supernatant solution was measured, which was relatively clear [39]. The higher the pH is, the greater the washout. When the AWCA dosage increased, the pH of the supernatant solution decreased. Before a dose of 0.6% was reached, the test results indicated that the washout resistance was affected, in order of importance, by the dosage of HPMC, PAM, PAC, and CMS (Figure 4) [40].

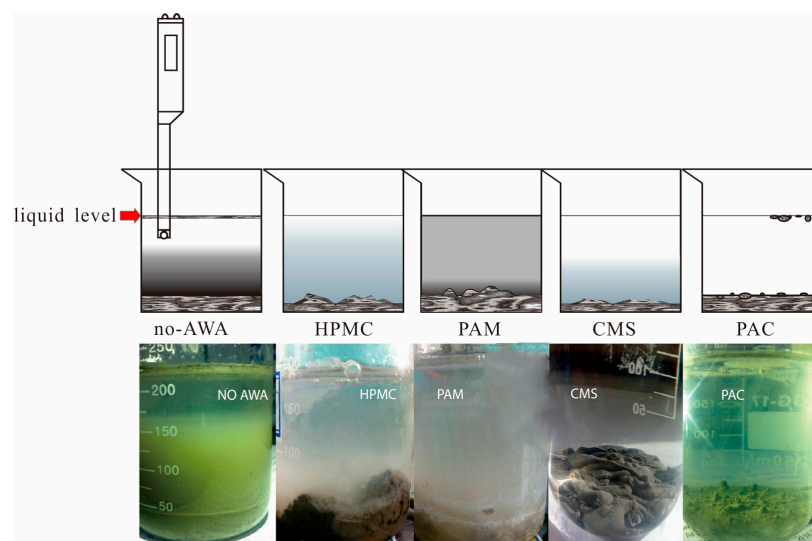


Figure 3. Flocculation states of cement paste with different AWAs.

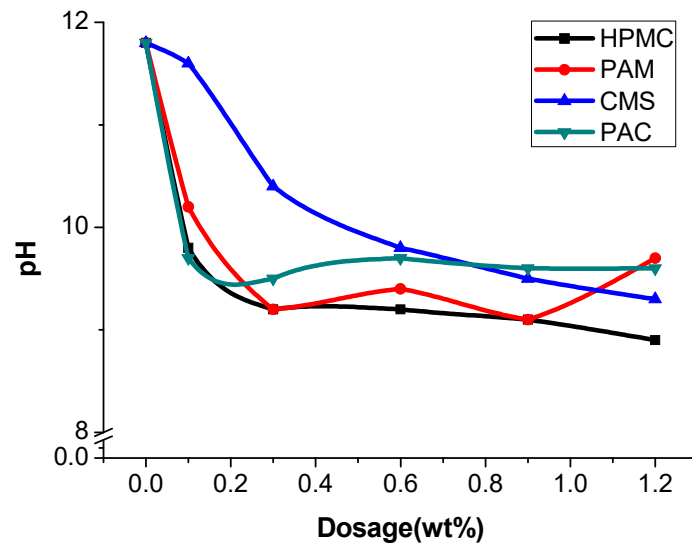


Figure 4. pH of the supernatant solution with different AWAs.

The stream test was first developed in Belgium. This method simulates the water flow and reduces the impact of the experimental error; thus, it is closer to the actual situation [41].

The test procedure involved the use of a 70 mm long guttering channel set at a slope of 15° to the horizontal (Figure 5). A sample of cement mortar was placed 300 mm from the raised end of the channel, and 100 mL of water was poured into the pipe three times [42]. Then, the mass loss of the mortar was measured. In addition, the pH of the turbid liquid was measured as a control.

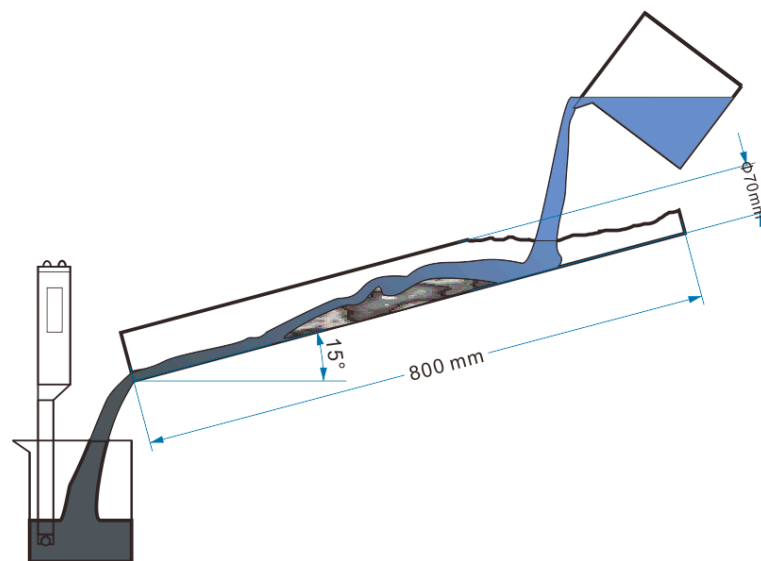


Figure 5. Stream test.

With an increase in the dosage of AWAs from 0 to 1.2%, the fluidity of the cement mortar sharply decreases, especially at low dosages. The curves plateau when the AWAs dose is greater than 0.6% (Figure 6), and the washout resistance of the cement mortars with these three kinds of AWAs is similar. However, before a dose of 0.6% was reached, the HPMC performed better.

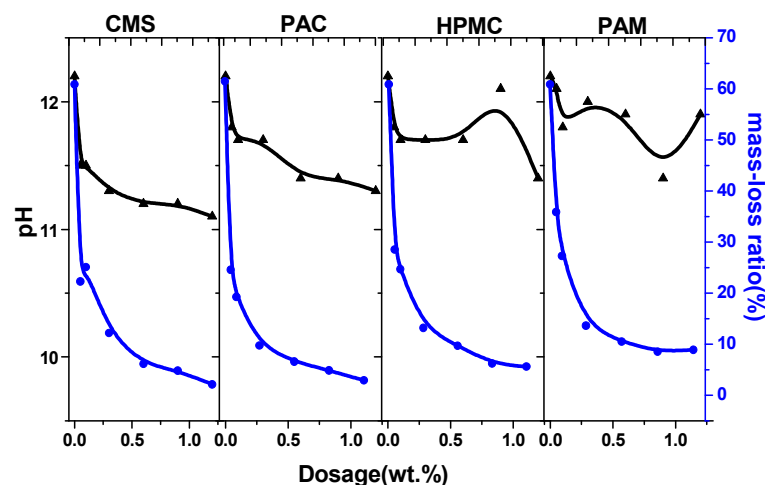


Figure 6. The mass loss and pH of cement paste with different AWAs. (The black lines represent changes in pH value, while the blue lines represent changes in mass loss).

For the comprehensive analysis of the results of the fluidity test and washout resistance test, the dosages of AWAs in the UWC were set at 0.1%, 0.3%, and 0.6%, and the mix proportions adopted for the UWC are listed in Table 2.

Table 2. The mix proportions of UWC.

W/C	Cement (kg/m ³)	Water (kg/m ³)	Sand (kg/m ³)	Aggregate (kg/m ³)		Superplasticizer (kg/m ³)
				2/16 mm	16/26.5 mm	
0.45	467	210	690	618	412	8.41

The change trends of the pH are similar to those of mass loss; however, the former are more unstable than the latter, which is mainly due to the differences in flocculation. Even though the supernatant of the cement slurry without AWAs was relatively clear, the pH was almost 12. Since there is no binding effect of AWA, Ca²⁺ and OH⁻ are more likely to spread easily from cement paste to water, and the suspension layer, which has a low strength after hardening, is also thicker [43]. The supernatants from AWAs are more turbid than those from other media, but because of the flocculation of AWAs, the cement particles are bound to the flocculation structure, increasing the difficulty of ion migration. Furthermore, the amount of these suspended particles was low; thus, the pH of the supernatant decreased. There are relatively large fluctuations in the pH of the samples with HPMC and PAM. The anionic groups in anionic AWAs adsorb cement particles to enhance flocculation, while the ionic AWAs can only fasten cement particles by adhering to a mass of spatial mesh structure. Therefore, ionic flocculation is poor and impedes cement hydration [44]. Overall, the linear correlation between pH and mass loss was greater for the sample with CMS than for the other samples, and the anionic AWAs were better and more stable than the ionic AWAs.

A comparison of the pH factor test and steam test results revealed that although they both had the same effect on the dosage of AWAs and had an anti-dispersion effect, the pH factor test was more unstable. In the horizontal comparison, the results of the steam test reflect the actual mass loss of the cement paste and more closely reflect the actual anti-dispersing ability of AWAs. The mass loss of paste with HPMC and PAM is greater than that with CMS and PAC. However, the results of the pH factor test are completely opposite to those of the steam test (Figure 5). The pH of the turbid liquids improved slightly but still deviated from the actual values.

2.4. Slump and Slump Flow of UWC

The slump and slump flow of the UWC were subsequently tested, and the results are presented in Table 3. (The slump is the vertical drop length, while the slump flow is the horizontal expansion diameter of the UWC).

Table 3. The slump and slump flow of UWC.

AWA-Dosage (%)		Non-AWA	HPMC	PAM	PAC	CMS
0.1	Slump	205	180	165	195	190
	Slump flow	345	275	...	290	300
0.3	Slump	205	150	145	165	185
	Slump flow	345	250	290
0.6	Slump	205	140	175
	Slump flow	345	275

At an AWA dosage of 0.6%, concrete with AWAs can hardly flow. Even at a dosage of 0.1%, the fluidity of the concrete was strongly impacted by the AWA, but bleeding or segregation did not occur. The comprehensive results show that slump and slump flow are affected, in order of importance, by PAM, HPMC, PAC, and CMS. Additionally, it is difficult for PAM to adapt to the mixing of concrete.

2.5. SEM Analysis of UWC

A certain amount of cement paste was taken during the process of UWC mixing, after which the samples were immediately dried and observed via SEM. The sample without AWAs started hydrating. There were thin layers of Aft and C-S-H gel on the surfaces of the cement particles (Figure 7) [45]. The sample with PAM also started hydrating but more slowly than the sample without AWA because the PAM network structures did not fully cover the cement particles and only the boundaries were covered, which resulted in hydration in the middle areas of the cement particles (Figure 8) [46]. The samples with HPMC, CMS, and PAC were almost not hydrated. Most of the cement particles were covered by AWAs, which caused a slow setting of the UWC. In addition, a large number of communication pores formed in the paste sample with HPMC (Figure 9), which may be the reason for its lower compressive strength. The influence of CMS and PAC on the pore structure is less than that of HPMC (Figures 10 and 11). Nonionic types like HPMC and PAM appeared to wrap around the cement grains, creating a physical barrier that retards dissolution and alters the hydration kinetics. This disruption in hydration can lead to heterogeneous microstructural development and potential defects. In contrast, anionic AWAs like CMS and PAC enabled particle binding without excessively coating surfaces, allowing for more regulated hydration and microstructure formation. These insights from SEM analysis inform the understanding of setting/hardening kinetics and mechanical property development in underwater concrete containing different AWAs. The main adhesion parts are the edges and the contact points between cement particles; therefore, they play positive roles in bridging cement paste. In summary, anionic AWAs can lead to slow UWC setting for wrapping effects, but they have less of an effect on the later hydration and pore structure. The ionic AWAs are denser and thicker than the anionic AWAs, and the fibers overlap each other to form well-like structures. A large number of communication pores are present in these structures. In addition, these well-like structures reduce the surface energy and formation energies of crystals of cement hydration products, thereby inducing the growth of crystals along these structures. In the end, the internal structures of the UWC change, and many harmful pores are formed.

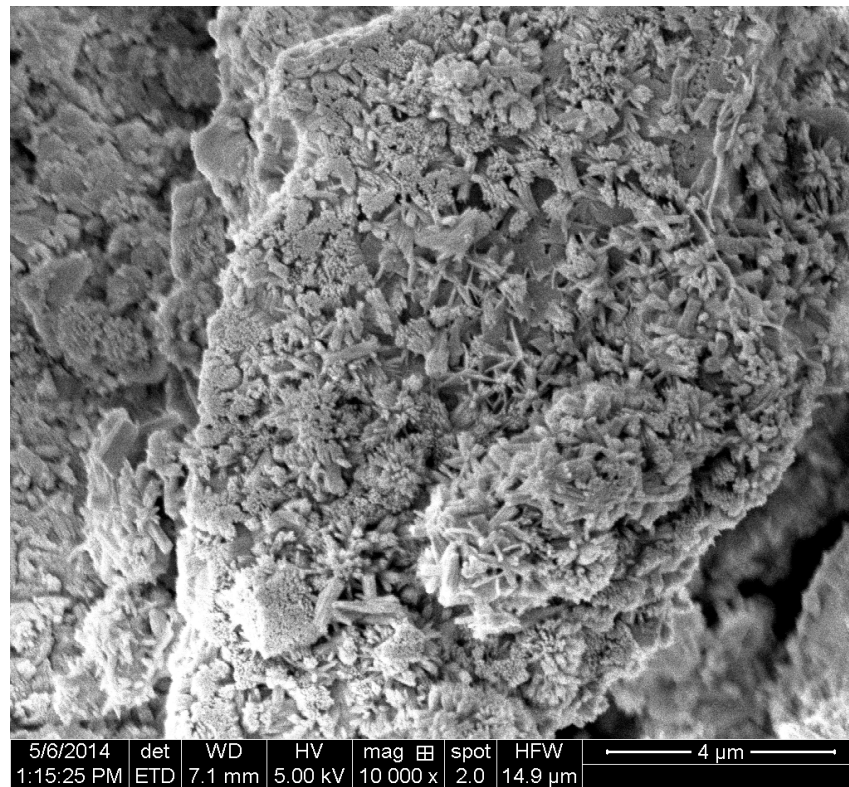


Figure 7. Scanning electron micrograph of the dried cement paste without AWAs.

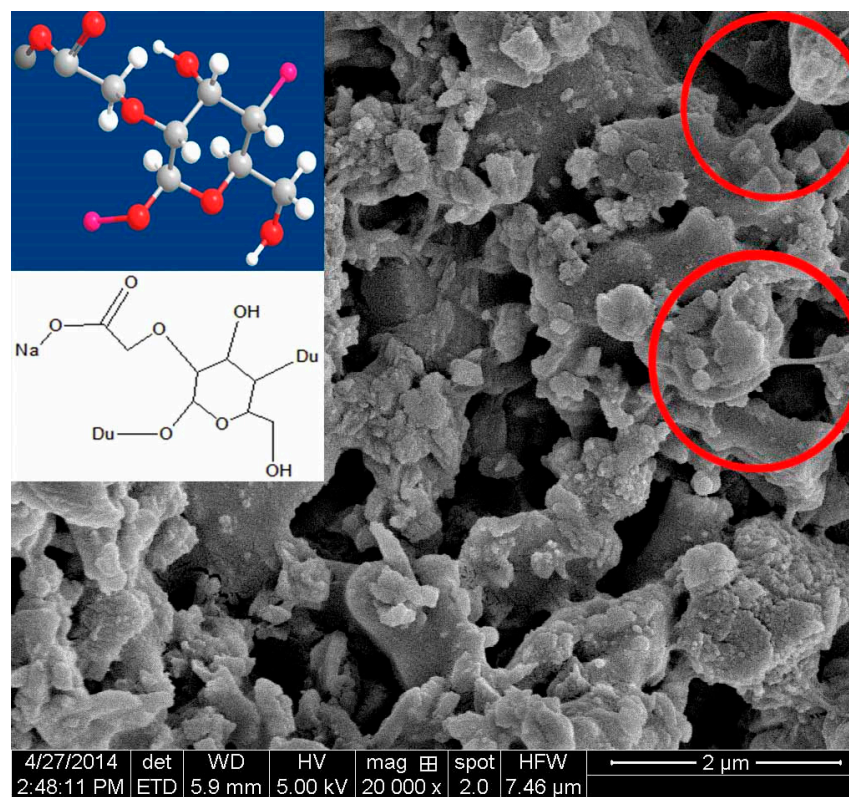


Figure 8. Scanning electron micrograph of the dried cement paste with CMS.

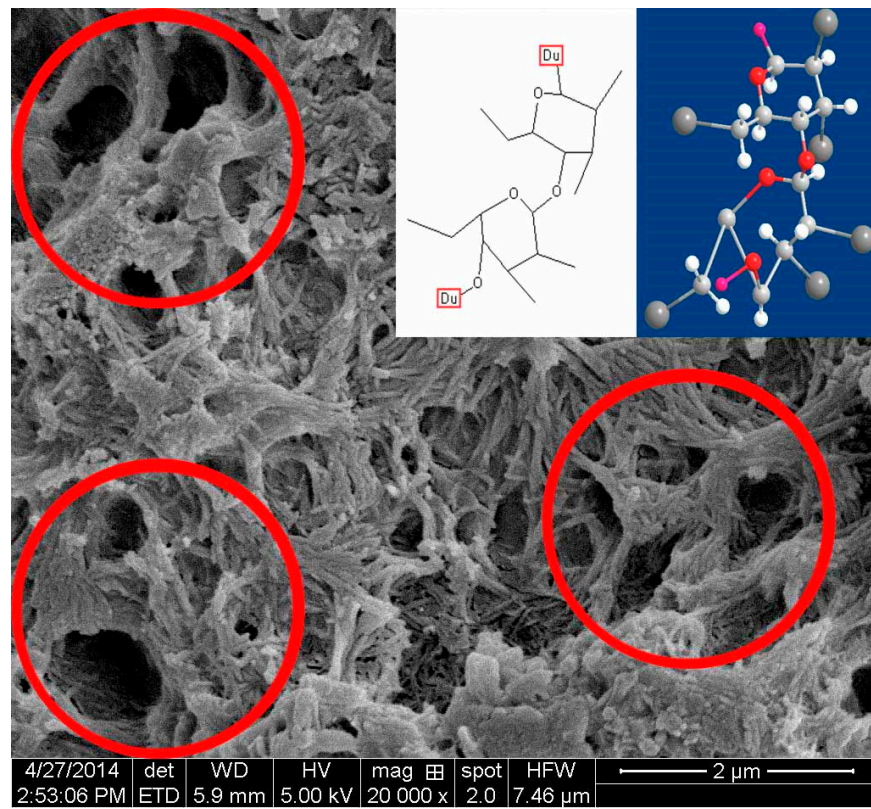


Figure 9. Scanning electron micrograph of the dried cement paste with HPMC.

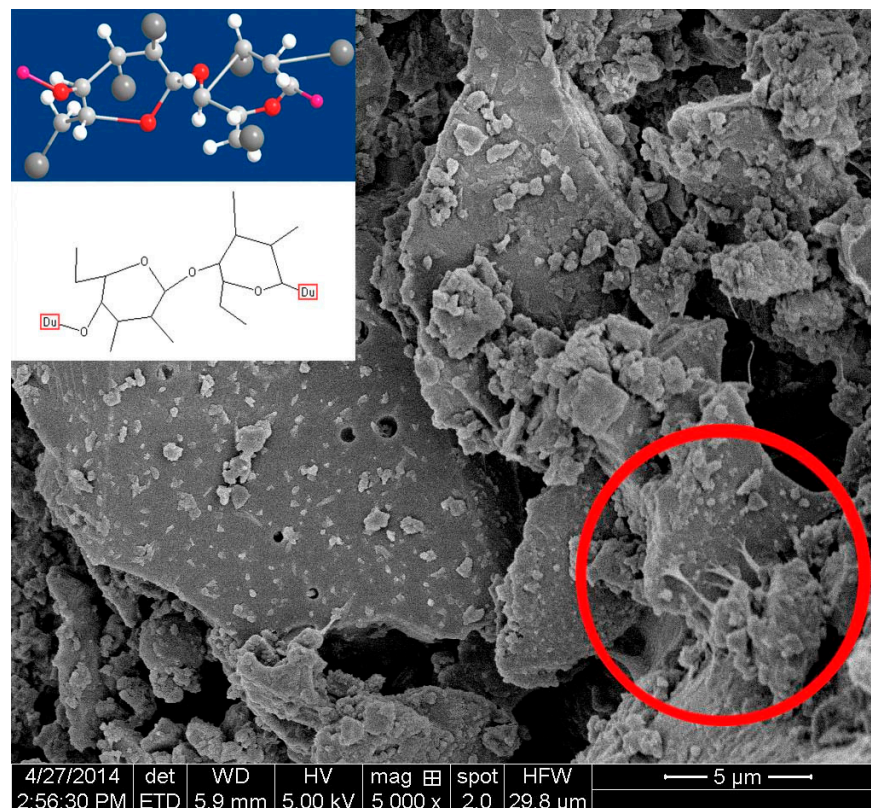


Figure 10. Scanning electron micrograph of the dried cement paste with PAC.

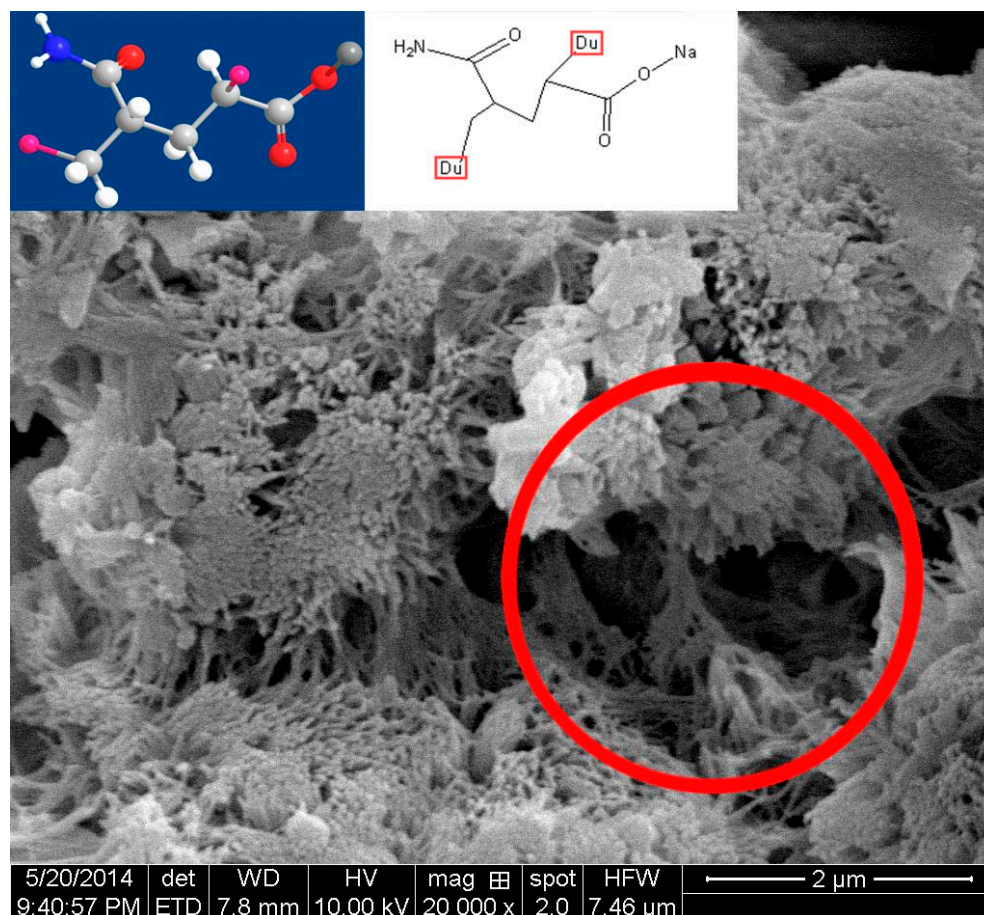


Figure 11. Scanning electron micrograph of the dried cement paste with PAM.

The network structures formed by HPMC demonstrate characteristic features of non-ionic association, enabled by hydrogen bonding between chains localized near particle surfaces. These intertwined polymeric matrices are looser and more open than anionic AWAs, as reflected by their high porosity and pore interconnectivity. Fluid transport through these networks is possible, even though diffusion is slowed. A subsequent strength reduction may arise as the networks remain partially intact during cement hydration, generating persistent flaws.

The extended fibrous morphology of the HPMC and related well-like structures suggest that the templates are capable of topologically guiding hydrate crystal growth. As demonstrated by analogous polymer–silica systems, the high-surface-area interfaces that are presented can thermodynamically stabilize certain crystal polymorphs and orientations while hindering others. The pores generated along such organic–inorganic composites thus have a high probability of persisting as flaws in the hardened cement matrix [47]. This finding illustrates how even ostensibly inert polymeric AWAs are capable of profoundly altering cement microstructures and developmental pathways.

Overall, integrating microscopic and nanoscopic tools such as SEM with tailored simulations and analytical models can substantially improve the mechanistic interpretations of macroscale AWA performance. These connections may catalyze the innovation of next-generation admixtures via the incorporation of molecular architecture considerations during their design. The spatial and temporal control of local interactions afforded by rational AWA engineering promises to unlock further possibilities for underwater concrete and construction.

2.6. Compressive Strength

Figures 12–14 show the compressive strength of the UWC with different dosages of AWAs. The Non and the Non (normal) are the controlled trials without AWAs, which are formed underwater, and the ordinary method, respectively. The early strength (3 days) of the UWC with AWAs is generally lower than that of those without AWAs (Figures 12–14), but the later strength is greater. With increasing AWA dosage, the strength decreases because of the negative effect of AWAs on the early hydration of cement.

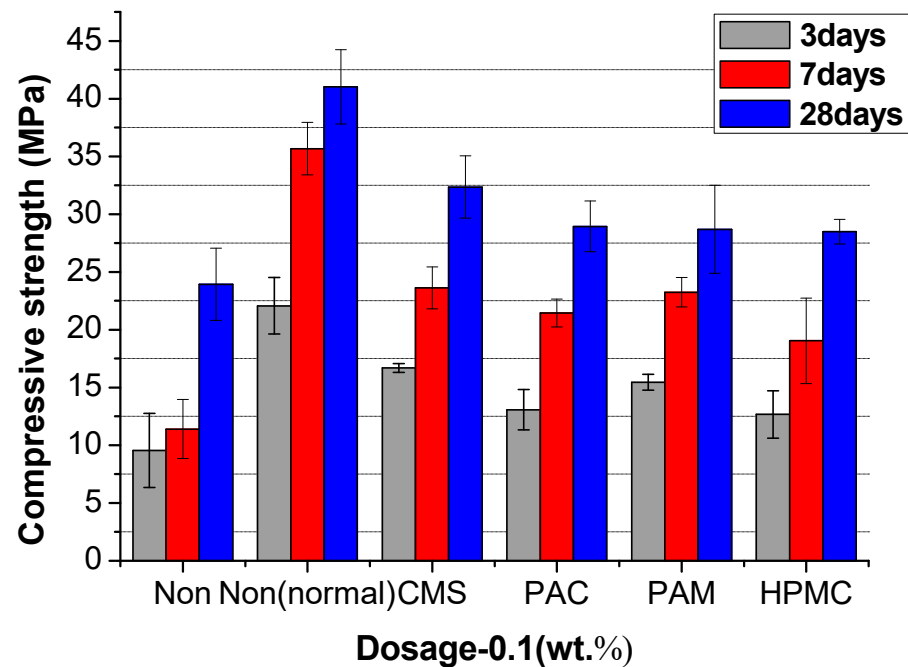


Figure 12. The compressive strength of UWC at an AWCA dosage of 0.1%.

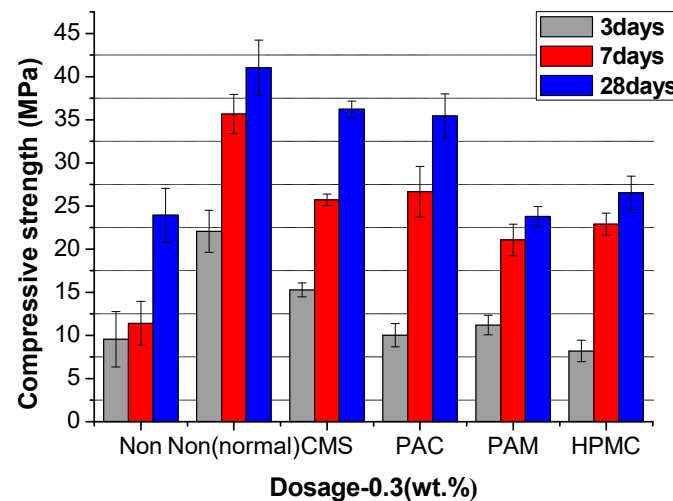


Figure 13. The compressive strength of UWC at an AWCA dosage of 0.3%.

The excessive network formation and high interhydroxide bonding of HPMC are reflected in the lowest later-age strength. The hydrogen-bonded chains likely remain partially intact during maturation, manifesting as flaws with a reduced load-bearing capacity. These persistent organic phases scattered among hydration products also disrupt matrix continuity and stress transfer. Conversely, the ionic bonding interactions of anionic AWAs appear less stable in high-pH pore fluid, enabling debonding and dissolution over time. The carboxyl groups of CMS, in particular, display an affinity for Ca^{2+} ions, initially

forming adsorbed surface layers. The subsequent complex fracture then exposes the particle surface to reaction progression. This eventual decrease in polymer barrier properties is consistent with the high late-age strength that is attained [48].

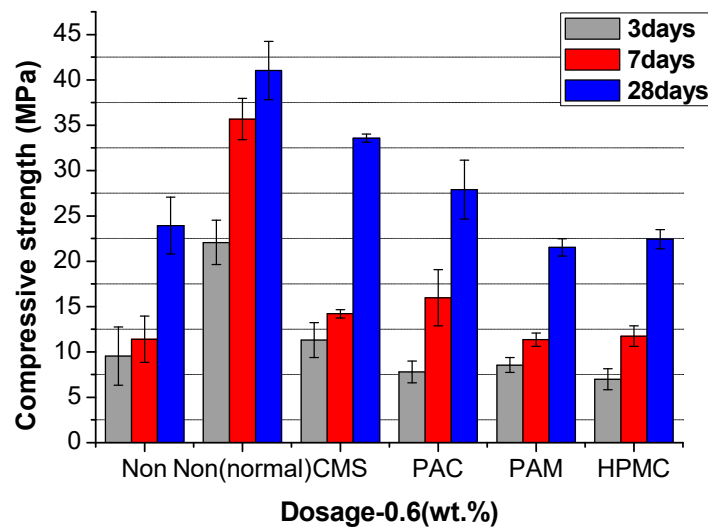


Figure 14. The compressive strength of UWC at an AWCA dosage of 0.6%.

By comparing PAC and CMS, the additional hydroxyl groups of the cellulosic CMS enabled greater initial hydration retardation from hydrogen bonding. This imparts a higher workability retention. However, the dual hydroxyl and carboxyl functionalities also introduce the competing effects of pore structure disruption and delayed debonding [49]. Optimizing this balance between early particle association and longer-term matrix incorporation is necessary for strength enhancement.

In summary, anionic AWAs exhibit superior strength development, attributable to their temporally regulated cement hydration. This contrasts with the uncontrolled pore structure modifications induced by nonionic stabilization [50]. Manipulating the ionic character and solubility of AWAs has emerged as a promising route for balancing the demands of underwater concrete rheology, setting, and structural performance.

2.7. Chemical Structures and Chemical Bonds of AWAs

The impacts of the molecular structure and polar groups of AWA on flocculation are quite different. These four kinds of AWAs are linear, but the length and shape of the molecular chains and functional groups dissociated in water are different. The length of the amide group in PAM is approximately 0.15 nm, the main chain is short, and the branched chain is longer, so the molecules are relatively tough. Moreover, there are $-\text{COOH}$ and $-\text{NH}_2$ groups, which have greater rigidity and toughness; therefore, PAM molecules have a greater influence on the fluidity of concrete. HPMC and PAC have the same main chain, but their functional groups are different. The molecular weight of HPMC is approximately 10,000–1,500,000 Da, the molecular chain can easily reunite to a ring form, and it appears as a beam-like structure with a collection of many monofilament fibers. Thus, the proportion of effective flocculation of HPCM is small; however, these structures affect the internal pore structures of concrete. Although PAC has the same main chain as HPMC, its molecular weight is only approximately 17,000 (when n is approximately 100). Therefore, the molecular chains of PAC are not easily intertwined, and the $-\text{CH}_2\text{COONa}$ on the glucose ring will repel PAC molecules with the same charge.

The molecular structure of CMS is different from that of the other CMSs (Figure 15). First, the main chain is short, but the branched chains are longer and softer because they are connected by single bonds, so the chains are easier to rotate. In addition, negative charges promote the dispersion of CMS, and flocculation structures are more likely to be net rather than linear. Therefore [51], the proportion of effective flocculation is greater.

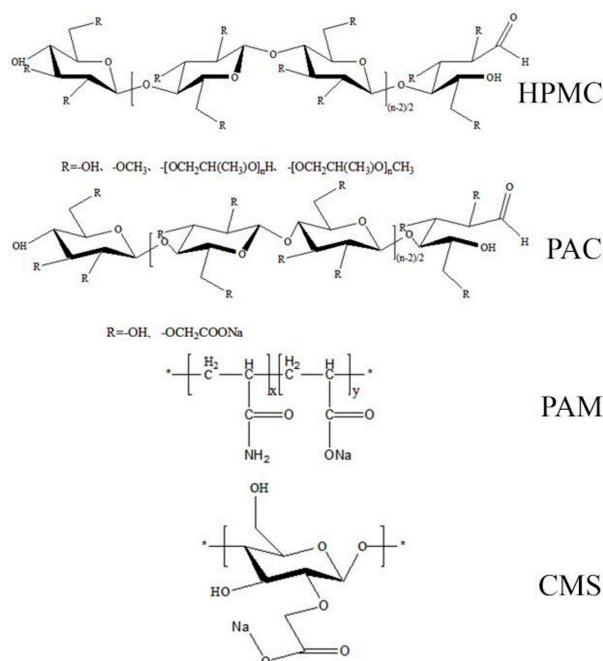


Figure 15. Chemical formulas of different AWAs. (The position of * means the starting and ending segments of each polymer repeating segment).

3. Molecular Dynamics Simulation

3.1. Model Construction

The CSH nanocone substrates were made of an ideal CSH model, namely, a tobermorite unit cell with a size of $22.32 \text{ \AA} \times 22.16 \text{ \AA} \times 22.77 \text{ \AA}$. First, the unit cell was enlarged 5 times along the z-direction, and part of the substrate was cleaved from the plane (0 0 1), leaving the C-S-H base located in the lower half (Figure 16). Then, the constructed AWAs were placed 5 \AA above the C-S-H substrate surface to ensure that organic molecules could be spontaneously adsorbed on the C-S-H substrate under natural conditions.

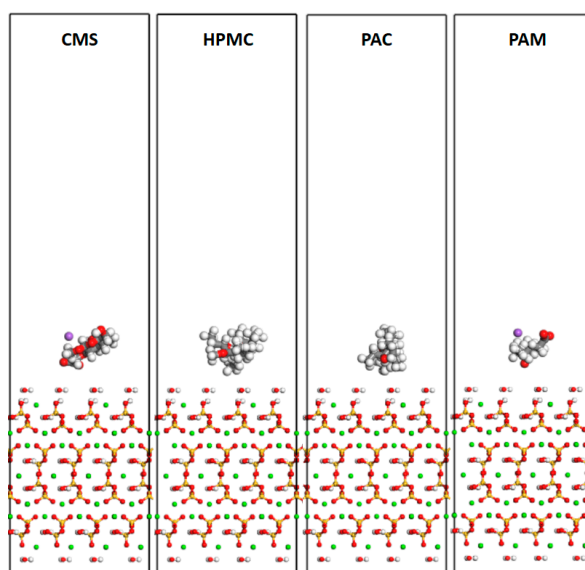


Figure 16. Models of the CMS, HPMC, PAC, and PAM systems.

3.2. Details

In this work, we used the ClayFF force field and CVFF force field [52] to simulate the interaction between C-S-H and the AWAs. Its accuracy has been proven for various cement hydrates and their interfaces.

LAMMPS (LAMMPS v1.2. <https://github.com/lammps/lammps> Release Stable release 2 August 2023, accessed on 14 March 2024), a large-scale molecular simulation software package, can simulate the molecular dynamics of organic–inorganic systems well. The whole simulation was run at a temperature of 300 K, a pressure of 1 atmosphere, and a time step of 1 fs. The whole system was under the NVT ensemble for 4 ns until the system reached equilibrium. The trajectory of atoms for the whole simulation was registered every 1 ps for data analysis [53].

3.3. Local Structure Analysis

The adsorption interactions between four AWAs and the major cement hydration product C-S-H were studied using molecular dynamics simulation methods, and the effects of additive functional groups on adsorption interactions were explained through simulation. First, the radial distribution function (RDF) curves between the atoms/ions of different molecular systems and the C-S-H interface were calculated. As shown in Figure 17a [54], there are obvious characteristic peaks within 2.45 Å between the CMS molecules and the C-S-H interface; these peaks are attributed to the interactions between the oxygen atoms in the organic molecules and the hydrogen atoms in the hydroxyl groups on the C-S-H surface. The peak value indicates that hydrogen bonds can be formed between them. The characteristic peak at 4 Å indicates that there are indirect interactions between them. In addition, the calcium ions in the C-S-H substrate can also form ionic interactions with the oxygen atoms in the molecules. However, compared with the results of previous studies, the position of this peak was slightly more biased toward the right side of the coordinate axis. This shows that the ionic interactions do not occur within the process range. The local structure is displayed in Figure 17b.

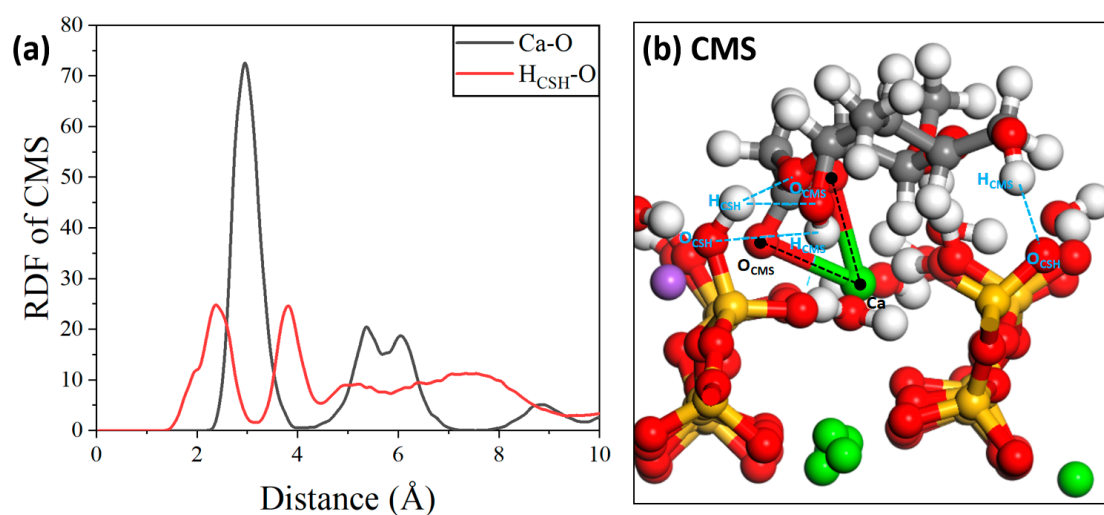


Figure 17. (a) RDF of CMS/C-S-H and (b) local structure.

For the HPMC molecules, the peak corresponding to hydrogen bonding occurred at 2 Å, indicating that the hydrogen bonding interactions between the HPMC molecules and the C-S-H substrate were more pronounced. For the mutual interaction between calcium cations, the RDF curves in Figure 18a show that the RDF peak value of Ca-O is located at approximately 4.8 Å, which far exceeds the range of Ca-O ionic interactions [55]. There are almost no short-range interactions between them. Therefore, the main interaction between the HPMC molecules and the C-S-H substrate is dominated by hydrogen bonding, and the interaction diagram is shown in Figure 18b.

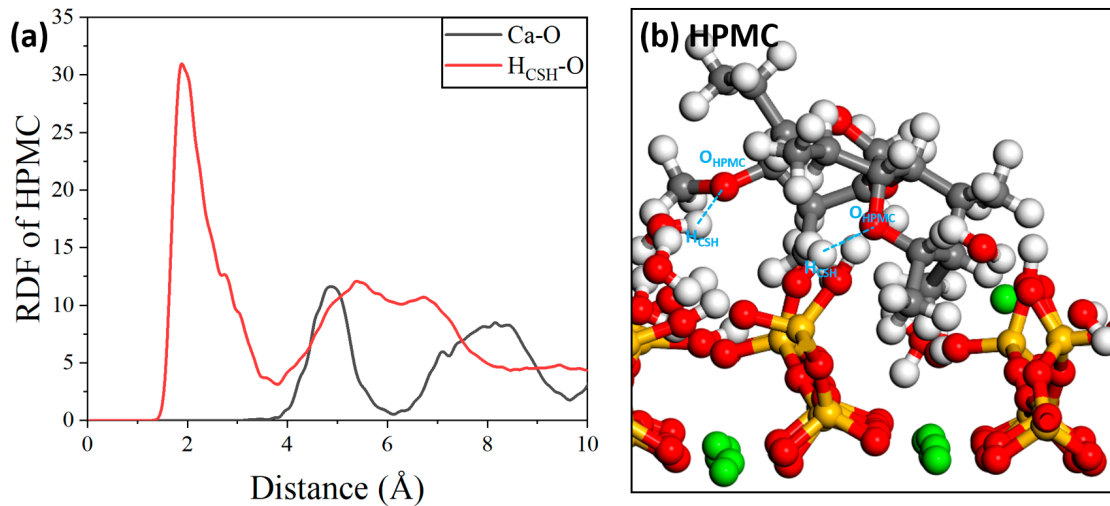


Figure 18. (a) RDF of HPMC/C-S-H and (b) local structure.

Regarding the interaction between PAC molecules and the C-S-H substrate, as shown in Figure 19a, similar to those between HPMC molecules and the C-S-H substrate, the mutual interaction between PAC molecules and the C-S-H substrate is also dominated by hydrogen bonding [56]. The ionic bonding range of Ca-O also far exceeded its theoretical range, indicating that there are similar indirect interactions between them. A schematic diagram of the intermolecular interactions is shown in Figure 19b.

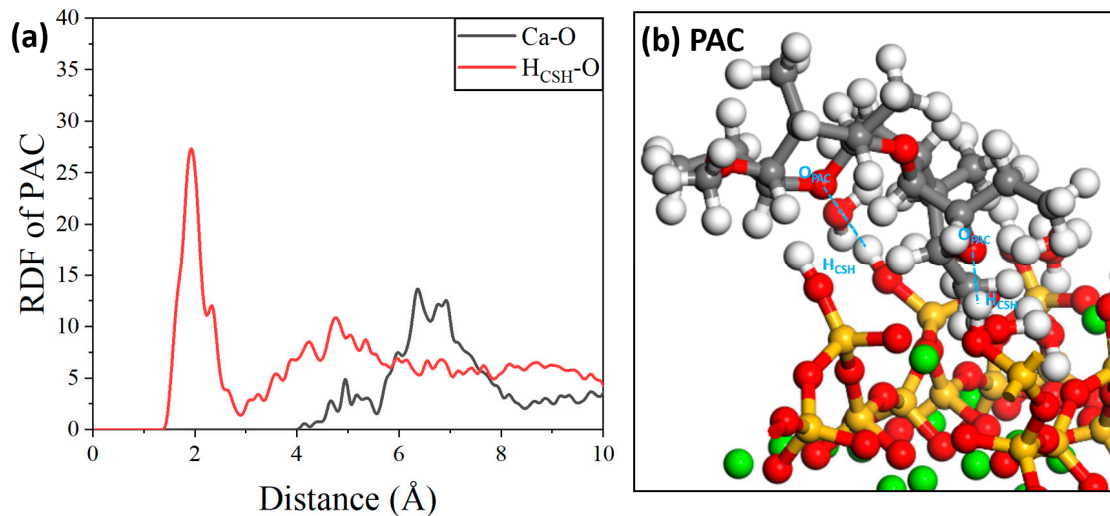


Figure 19. (a) RDF of PAC/C-S-H and (b) local structure.

Finally, as shown in Figure 20, regarding the interaction between the PAM molecule and the C-S-H substrate, first, the oxygen atom in the PAM molecule can effectively form a Ca-O ionic interaction with the calcium ion in the C-S-H substrate. In addition, for the point interaction, there is an obvious peak within 2.4 Å, which is the hydrogen bonding range, indicating that there could also be hydrogen bonding interactions between them, and the shoulder peak near 4 Å shows that PAM molecules can effectively form close-range hydrogen bonds with the hydrogen atoms in the C-S-H substrate. The interactions between the PAM molecules and the C-S-H substrate are richer in form and stronger in intensity [57].

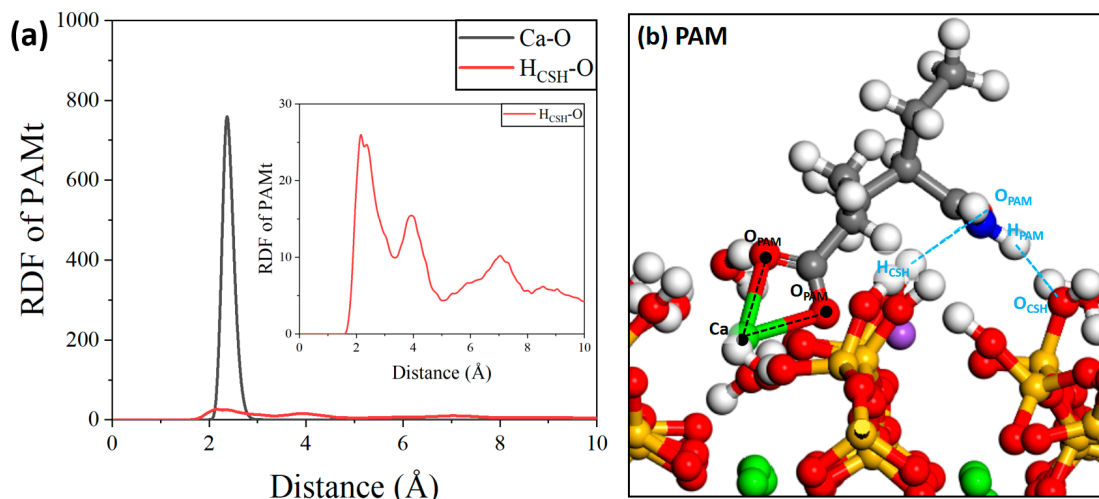


Figure 20. (a) RDF of PAM/C-S-H and (b) local structure.

4. Conclusions

This comparative study between nonionic and anionic AWAs revealed significant differences in performance, attributable to the underlying interaction mechanisms with cementitious systems.

- (1) Compared with extensive surface adsorption, anionic AWAs demonstrate less deterioration in terms of workability owing to the interparticle binding locations for nonionic variants. The hydrogen-bonded networks formed by nonionic AWAs also disrupt pore structure development and hydration kinetics. These effects persist, manifesting in substantial late-age strength reductions.
- (2) Conversely, the ionic bonding of anionic AWAs appears more temporally regulated, with delayed debonding enabling hydration progression. The carboxyl–hydroxyl functionalities provide an optimal balance between early flocculation and longer-term matrix incorporation.
- (3) While nonionic AWAs exhibit stability due to their viscous entangled associations, particulate systems are prone to flow-induced disruption without stabilizing particle charges. Compared with condensed anionic landscapes, looser polymer assemblies also risk contaminant transport.
- (4) Anionic AWAs exhibit superior performance for underwater concrete because of their balanced rheology, cohesion, reduced defects, and ultimate strength. Further innovations targeting the ionic character, solubility, and nano-to-microscale interactions of AWA with cement promise continued advancements. According to the fluidity test, the average fluidity decreases by 45.1% and 37.5% with nonionic and anionic AWAs, respectively, which shows that anionic AWAs have a less negative impact on the flow properties of concrete.

Author Contributions: Conceptualization, X.S. and L.X.; methodology, X.S.; software, X.S.; validation, X.S., H.Z. and T.X.; formal analysis, X.S.; investigation, Q.L.; resources, X.S.; data curation, X.S.; writing—original draft preparation, X.S.; writing—review and editing, L.X.; visualization, T.X.; supervision, L.X.; project administration, L.X.; funding acquisition, H.Z. All authors have read and agreed to the published version of the manuscript.

Funding: This research received no external funding.

Data Availability Statement: The original contributions presented in the study are included in the article, further inquiries can be directed to the corresponding authors.

Acknowledgments: Special thanks to Bo Pang from the Department of Civil Engineering, Qingdao University of Technology for his help in chemical synthesis.

Conflicts of Interest: The authors declare no conflict of interest.

References

1. Lu, H.; Sun, X.; Ma, H. Anti-washout concrete: An overview. *Constr. Build. Mater.* **2022**, *344*, 128151. [CrossRef]
2. Yu, Z.; Wang, B.; Li, T.; Wang, W. The anti-dispersion mechanism of polyacrylamide on alkali-activated cementitious materials poured underwater. *Constr. Build. Mater.* **2024**, *414*, 134958. [CrossRef]
3. Assaad, J.J.; Gerges, N.; Khayat, K.H.; Lattouf, N.; Mansour, J. Assessment of bond strength of underwater polymer-modified concrete. *ACI Mater. J.* **2019**, *116*, 169–178. [CrossRef]
4. Sun, Z.; Li, Y.; Ming, X.; Chen, B.; Li, Z. Enhancing anti-washout behavior of cement paste by polyacrylamide gelation: From flocc properties to mechanism. *Cem. Concr. Compos.* **2023**, *136*, 104887. [CrossRef]
5. Lu, H.; He, Y.; Jiang, T.; Xu, F.; Wei, H.; Xiang, J. Anti-Washout Mechanism of Underwater Cement Paste: A DEM-CFD Coupling Analysis Method. Available online: <https://ssrn.com/abstract=4604228> (accessed on 17 October 2023).
6. Yuan, Q.; Xie, Z.; Yao, H.; Huang, T.; Fan, M. Hydration, mechanical properties, and microstructural characteristics of cement pastes with different ionic polyacrylamides: A comparative study. *J. Build. Eng.* **2022**, *56*, 104763. [CrossRef]
7. Yuan, Q.; Xie, Z.; Yao, H.; Fan, M.; Huang, T. Comparative study on the early properties of cement modified with different ionic polyacrylamides. *Constr. Build. Mater.* **2022**, *339*, 127671. [CrossRef]
8. Gelardi, G.; Mantellato, S.; Marchon, D.; Palacios, M.; Eberhardt, A.; Flatt, R. Chemistry of chemical admixtures. In *Science and Technology of Concrete Admixtures*; Elsevier: Amsterdam, The Netherlands, 2016; pp. 149–218.
9. Bessaies-Bey, H.; Khayat, K.H.; Palacios, M.; Schmidt, W.; Roussel, N. Viscosity modifying agents: Key components of advanced cement-based materials with adapted rheology. *Cem. Concr. Res.* **2022**, *152*, 106646. [CrossRef]
10. Barbhuiya, S.; Das, B.B. Water-soluble polymers in cementitious materials: A comprehensive review of roles, mechanisms and applications. *Case Stud. Constr. Mater.* **2023**, *19*, e02312. [CrossRef]
11. Han, B.; Zhang, L.; Ou, J. *Smart and Multifunctional Concrete toward Sustainable Infrastructures*; Springer: Berlin/Heidelberg, Germany, 2017.
12. Zhang, Q.; Chen, J.; Zhu, J.; Yang, Y.; Zhou, D.; Wang, T.; Shu, X.; Qiao, M. Advances in Organic Rheology-Modifiers (Chemical Admixtures) and Their Effects on the Rheological Properties of Cement-Based Materials. *Materials* **2022**, *15*, 8730. [CrossRef]
13. Zheng, H.; Pang, B.; Jin, Z.; Liu, S.; Zhang, Y.; Bi, J.; Chang, H.; Liu, Y.; Wang, F. Mechanical properties and microstructure of waterborne polyurethane-modified cement composites as concrete repair mortar. *J. Build. Eng.* **2024**, *84*, 108394. [CrossRef]
14. Bessaies-Bey, H.; Baumann, R.; Schmitz, M.; Radler, M.; Roussel, N. Effect of polyacrylamide on rheology of fresh cement pastes. *Cem. Concr. Res.* **2015**, *76*, 98–106. [CrossRef]
15. Cano-Barrita, P.d.J.; León-Martínez, F. *Biopolymers with Viscosity-Enhancing Properties for Concrete, Biopolymers and Biotech Admixtures for Eco-Efficient Construction Materials*; Elsevier: Amsterdam, The Netherlands, 2016; pp. 221–252.
16. Ohama, Y. *Handbook of Polymer-Modified Concrete and Mortars: Properties and Process Technology*; William Andrew: Norwich, NY, USA, 1995.
17. Yuan, Q.; Liu, W.-t.; Wang, C.; Deng, D.-h.; Liu, Z.-q.; Long, G.-c. Coupled effect of viscosity enhancing admixtures and superplasticizers on rheological behavior of cement paste. *J. Cent. South Univ.* **2017**, *24*, 2172–2179. [CrossRef]
18. González-Aviña, J.; Hosseinpour, M.; Yahia, A.; Durán-Herrera, A. New biopolymers as viscosity-modifying admixtures to improve the rheological properties of cement-based materials. *Cem. Concr. Compos.* **2024**, *146*, 105409. [CrossRef]
19. Xiang, S.; Tan, Y.; Gao, Y.; Jiang, Z.; Liu, B.; Zeng, W. Bubble Evolution under the Action of Polycarboxylate and Air-Entraining Agent and Its Effects on Concrete Properties—A Review. *Materials* **2022**, *15*, 7053. [CrossRef]
20. Jiang, C.; Liu, J.; Liu, L.; Chen, Z.; Shi, C. Interactions between coral sand and polycarboxylate superplasticizer and their effects on rheological properties of cement-based materials—A review. *Constr. Build. Mater.* **2023**, *389*, 131607. [CrossRef]
21. Pang, B.; Zheng, H.; Jin, Z.; Hou, D.; Zhang, Y.; Song, X.; Sun, Y.; Liu, Z.; She, W.; Yang, L. Inner superhydrophobic materials based on waste fly ash: Microstructural morphology of microetching effects. *Compos. Part B Eng.* **2024**, *268*, 111089. [CrossRef]
22. Islam, M. Feasibility of Making Aircrete without Autoclave Using Indigenous Materials in Bangladesh. Master's Thesis, Bangladesh University of Engineering and Technology, Dhaka, Bangladesh, 2011.
23. Badry, F. Experimental and Numerical Studies in Self-Compacting Concrete. Ph.D. Thesis, Cardiff University, Cardiff, UK, 2015.
24. Deeb, R. Flow of Self-Compacting Concrete. Ph.D. Thesis, Cardiff University, Cardiff, UK, 2013.
25. Knapen, E. Microstructure Formation in Cement Mortars Modified with Water-Soluble Polymers (Microstructuurpobouw bij Cementmortels Gemodificeerd met Wateroplosbare Polymeren). Ph.D. Thesis, Katholieke Universiteit Leuven, Leuven, Belgium, 2007.
26. Hou, D.; Yang, Q.; Wang, P.; Jin, Z.; Wang, M.; Zhang, Y.; Wang, X. Unraveling disadhesion mechanism of epoxy/CSH interface under aggressive conditions. *Cem. Concr. Res.* **2021**, *146*, 106489. [CrossRef]
27. Pang, B.; Jin, Z.; Zhang, Y.; Liu, Z.; She, W.; Wang, P.; Yu, Y.; Zhang, X.; Xiong, C.; Li, N. Ultraductile cementitious structural health monitoring coating: Waterborne polymer biomimetic muscle and polyhedral oligomeric silsesquioxane-assisted C-S-H dispersion. *Adv. Funct. Mater.* **2022**, *32*, 2208676. [CrossRef]
28. Wu, Z.; Lin, Z.; Yao, A.; Ye, S.; Pan, H.; Cui, X.; Wang, D. Influence of particle size distribution on the rheological properties and mathematical model fitting of injectable borosilicate bioactive glass bone cement. *Ceram. Int.* **2020**, *46*, 24395–24406. [CrossRef]

29. Li, X.; Li, G.; Zhang, K.; Pei, Z.; Zhao, S.; Li, J. Cu-loaded Brushite bone cements with good antibacterial activity and operability. *J. Biomed. Mater. Res. Part B Appl. Biomater.* **2021**, *109*, 877–889. [[CrossRef](#)]
30. Pang, B.; Zhou, Z.; Xu, H. Utilization of carbonated and granulated steel slag aggregate in concrete. *Constr. Build. Mater.* **2015**, *84*, 454–467. [[CrossRef](#)]
31. Li, C.; Hao, W.; Wu, C.; Li, W.; Tao, J.; Ai, F.; Xin, H.; Wang, X. Injectable and bioactive bone cement with moderate setting time and temperature using borosilicate bio-glass-incorporated magnesium phosphate. *Biomed. Mater.* **2020**, *15*, 045015. [[CrossRef](#)] [[PubMed](#)]
32. Lin, M.-C.; Chen, C.-C.; Wu, I.-T.; Ding, S.-J. Enhanced antibacterial activity of calcium silicate-based hybrid cements for bone repair. *Mater. Sci. Eng. C* **2020**, *110*, 110727. [[CrossRef](#)] [[PubMed](#)]
33. Kumar, B.G.; Muthu, M.; Chajec, A.; Sadowski, Ł.; Govindaraj, V. The effect of silica fume on the washout resistance of environmentally friendly underwater concrete with a high-volume of siliceous fly ash. *Constr. Build. Mater.* **2022**, *327*, 127058. [[CrossRef](#)]
34. Pang, B.; Jia, Y.; Pang, S.D.; Zhang, Y.; Du, H.; Geng, G.; Ni, H.; Qian, J.; Qiao, H.; Liu, G. The interpenetration polymer network in a cement paste–waterborne epoxy system. *Cem. Concr. Res.* **2021**, *139*, 106236. [[CrossRef](#)]
35. Gelli, R.; Bernardini, G.; Ridi, F. Strontium-loaded magnesium phosphate bone cements and effect of polymeric additives. *Ceram. Int.* **2023**, *49*, 31466–31476. [[CrossRef](#)]
36. Al-Saffar, D.M.; Al-Shathr, B.S.; Abed, S.K. Evaluating Fresh Properties of Non-Dispersive Reactive Powder Concrete: A Novel Approach. *Math. Model. Eng. Probl.* **2023**, *10*, 1324. [[CrossRef](#)]
37. Jeon, I.K.; Qudoos, A.; Woo, B.H.; Yoo, D.H.; Kim, H.G. Effects of nano-silica and reactive magnesia on the microstructure and durability performance of underwater concrete. *Powder Technol.* **2022**, *398*, 116976. [[CrossRef](#)]
38. Pang, B.; Zhou, Z.; Hou, P.; Du, P.; Zhang, L.; Xu, H. Autogenous and engineered healing mechanisms of carbonated steel slag aggregate in concrete. *Constr. Build. Mater.* **2016**, *107*, 191–202. [[CrossRef](#)]
39. Zhang, K.; Li, G.; Pei, Z.; Zhao, S.; Jing, A.; Liang, G. Injectable graphite-modified Fe₃O₄/calcium phosphate bone cement with enhanced heating ability for hyperthermia. *Mater. Technol.* **2020**, *35*, 863–871. [[CrossRef](#)]
40. Pei, Z.; Zhang, Z.; Li, G.; Fu, F.; Zhang, K.; Cai, Y.; Yang, Y. Improvement of in vitro osteogenesis and antimicrobial activity of injectable brushite for bone repair by incorporating with Se-loaded calcium phosphate. *Ceram. Int.* **2021**, *47*, 11144–11155. [[CrossRef](#)]
41. Sogbe, M.; López-Guerra, D.; Blanco-Fernández, G.; Sangro, B.; Narváez-Rodríguez, I. Durvalumab as a successful downstaging therapy for liver transplantation in hepatocellular carcinoma: The importance of a washout period. *Transplantation* **2021**, *105*, e398–e400. [[CrossRef](#)]
42. Nasr, A.A.; Chen, S.; Wang, Y.; Jin, F.; Qiu, L.-C. Strength evaluation of a new underwater concrete type. *Case Stud. Constr. Mater.* **2022**, *16*, e00884. [[CrossRef](#)]
43. Pang, B.; Zhou, Z.; Cheng, X.; Du, P.; Xu, H. ITZ properties of concrete with carbonated steel slag aggregate in salty freeze-thaw environment. *Constr. Build. Mater.* **2016**, *114*, 162–171. [[CrossRef](#)]
44. Honda, M.; Kawanobe, Y.; Nagata, K.; Ishii, K.; Matsumoto, M.; Aizawa, M. Bactericidal and bioresorbable calcium phosphate cements fabricated by silver-containing tricalcium phosphate microspheres. *Int. J. Mol. Sci.* **2020**, *21*, 3745. [[CrossRef](#)] [[PubMed](#)]
45. Liu, J.-Q.; Yuen, K.-V.; Chen, W.-Z.; Zhou, X.-S. Grouting for water and mud inrush control in weathered granite tunnel: A case study. *Eng. Geol.* **2020**, *279*, 105896. [[CrossRef](#)]
46. Pang, B.; Zhang, Y.S.; Liu, G.J. Study on the effect of waterborne epoxy resins on the performance and microstructure of cement paste. *Constr. Build. Mater.* **2018**, *167*, 831–845. [[CrossRef](#)]
47. Pang, B.; Liu, Y.; Wang, P.; Tian, L.; Song, X.; Zhang, W. Composite Hydrophobic Coatings with Progressive High Penetration through Chromatography: Protective Properties and Mechanisms. *ACS Appl. Polym. Mater.* **2024**. [[CrossRef](#)]
48. Liu, Z.; Jiang, J.; Jin, X.; Wang, Y.; Zhang, Y. Experimental and numerical investigations on the inhibition of freeze–thaw damage of cement-based materials by a methyl laurate/diatomite microcapsule phase change material. *J. Energy Storage* **2023**, *68*, 107665. [[CrossRef](#)]
49. Pang, B.; Zhang, Y.; Liu, G.; She, W. Interface properties of nanosilica-modified waterborne epoxy cement repairing system. *ACS Appl. Mater. Interfaces* **2018**, *10*, 21696–21711. [[CrossRef](#)]
50. Liu, Z.; Qian, R.; Gao, S.; Wang, Y.; Jiang, J.; Zhang, Y. Modelling of Damage Spatiotemporal Distribution in Saturated Cementitious Materials and its Chloride Transport Evolution. *J. Adv. Concr. Technol.* **2023**, *21*, 248–261. [[CrossRef](#)]
51. Pang, B.; Qian, J.; Zhang, Y.; Jia, Y.; Ni, H.; Pang, S.D.; Liu, G.; Qian, R.; She, W.; Yang, L.; et al. 5S Multifunctional Intelligent Coating with Superdurable, Superhydrophobic, Self-Monitoring, Self-Heating, and Self-Healing Properties for Existing Construction Application. *ACS Appl. Mater. Interfaces* **2019**, *11*, 29242–29254. [[CrossRef](#)]
52. Pang, B.; Jin, Z.; Zhang, Y.; Xu, L.; Li, M.; Wang, C.; Zhang, Y.; Yang, Y.; Zhao, P.; Bi, J. Ultraductile waterborne epoxy-concrete composite repair material: Epoxy-fiber synergistic effect on flexural and tensile performance. *Cem. Concr. Compos.* **2022**, *129*, 104463. [[CrossRef](#)]
53. Pang, B.; Jia, Y.T.; Zhang, Y.S.; Ni, H.M.; Liu, G.J.; She, W.; Yang, L.; Qian, R.S. Effect of the combined treatment with inorganic and organic agents on the surface hardening and adhesion properties of cement-based materials. *Mater. Des.* **2019**, *169*, 107673. [[CrossRef](#)]

54. Hou, D.; Zheng, H.; Wang, P.; Wan, X.; Yin, B.; Wang, M.; Zhang, J. Molecular dynamics study on sodium chloride solution transport through the Calcium-Silicate-Hydrate nanocone channel. *Constr. Build. Mater.* **2022**, *342*, 128068. [[CrossRef](#)]
55. Hou, D.; Zhang, W.; Sun, M.; Wang, P.; Wang, M.; Zhang, J.; Li, Z. Modified Lucas-Washburn function of capillary transport in the calcium silicate hydrate gel pore: A coarse-grained molecular dynamics study. *Cem. Concr. Res.* **2020**, *136*, 106166. [[CrossRef](#)]
56. Pang, B.; Jia, Y.; Pang, S.D.; Zhang, Y.; Du, H.; Geng, G.; Ni, H.; Qian, J.; Qiao, H.; Yang, L.; et al. Research on the toughening mechanism of modified nano-silica and silane molecular cages in the multi-scale microfracture of cement-epoxy composite. *Cem. Concr. Compos.* **2021**, *119*, 104027. [[CrossRef](#)]
57. Jin, Z.; Li, M.; Pang, B.; Yang, L.; Chen, Y.; Wang, D. Internal superhydrophobic marine concrete: Interface modification based on slag microstructure regulation. *J. Build. Eng.* **2024**, *86*, 108769. [[CrossRef](#)]

Disclaimer/Publisher's Note: The statements, opinions and data contained in all publications are solely those of the individual author(s) and contributor(s) and not of MDPI and/or the editor(s). MDPI and/or the editor(s) disclaim responsibility for any injury to people or property resulting from any ideas, methods, instructions or products referred to in the content.